In situ Phase Analysis of the Thermal Decomposition Products of Zirconium Salts*

Goran Štefanić,[a,**] *Biserka Gržeta,*[a] *Stanko Popović,*[b] *and Svetozar Musić* [a]

[a] *Ruđer Bošković Institute, P. O. Box 1016, 10001 Zagreb, Croatia*

[b] *Department of Physics, Faculty of Science, University of Zagreb, P. O. Box 162, 10001 Zagreb, Croatia*

X-ray powder diffraction at high temperature was used to determine the phase composition of the thermal decomposition products of two zirconium salts, $Zr(SO_4)_2 \cdot 4 H_2O$ and $ZrO(NO_3)_2 \cdot 2 H_2O$, and of a mixture of zirconium nitrates having $Zr(OH)_2(NO_3)_2 \cdot 4.7 H_2O$ and $ZrO(NO_3)_2 \cdot 2 H_2O$ as dominant components. Heating of the samples up to 1200 °C was performed inside a high-temperature chamber, attached to a diffractometer, at an air pressure of $\approx 2 \times 10^{-3}$ Pa. Regardless of the structural differences in the starting salts, thermal decomposition products crystallized to t-ZrO_2, which remained stable up to 1200 °C. This result indicated that the structural nature of the starting materials was not the most important factor of metastable t-ZrO_2 formation. The thermodynamically stable m-ZrO_2 appeared after the cooling of the samples to room temperature. If the cooling was performed at low air pressure, the m-ZrO_2 content was small. Introduction of air, even at RT, caused a considerable increase of m-ZrO_2, which became the dominant phase in all cases. The important role of oxygen in the t-$ZrO_2 \rightarrow m$-ZrO_2 transition indicates that the lack of oxygen in the zirconia lattice favours the formation of metastable t-ZrO_2.

Key words: t-ZrO_2, m-ZrO_2, X-ray diffraction, *in situ* phase analysis, phase transitions, lattice defects.

---

* Dedicated to Professor Boris Kamenar on the occasion of his 70th birthday.

** Author to whom correspondence should be addressed. (E-mail: stefanic@rudjer.irb.hr)

INTRODUCTION

The appearance of metastable tetragonal zirconia, t-ZrO_2, a product of thermal decomposition of zirconium salt, $ZrOCl_2 \cdot 8\,H_2O$, was first reported by Clark and Reynolds.[1] The same authors[1] observed the presence of t-ZrO_2 in the crystallization product of hydrous zirconia, obtained after calcination at 500 °C. The reason for the formation of this high temperature polymorph (thermodynamically stable above 1170 °C) at room temperature is still a matter of controversy. Several proposed models emphasized the role of anionic impurities (SO_4^{2-}, OH^-),[2–4] crystallite size (surface energy),[5–7] structural similarities between the starting material and t-ZrO_2,[8–10] lattice strains[11], water vapour,[12,13] lattice defects (oxygen vacancies),[14,15] pH and time of hydrous zirconia precipitation,[16] *etc*. Most of these models were based on results obtained from investigations of the crystallization products of hydrous zirconia.[2–4,8–16] The preparation conditions used to obtain hydrous zirconia precursors strongly influence the phase composition of the ZrO_2 crystallization products. The formation and the fraction of metastable t-ZrO_2 depends on the pH,[17] time of precipitation,[18] nature of the starting salt[19] and the mechanical treatment[20] applied during the processing of hydrous zirconia precursors. The amorphous nature of hydrous zirconia precursor makes the investigation of the mechanism of t-ZrO_2 formation even more complex. Livage *et al.*[8] concluded that the local atomic arrangement in amorphous zirconia (Zr–Zr and Zr–O distances) is similar to that of t-ZrO_2. On the other hand, the more recent investigations of Zang *et al.*[21] and Yanwei *et al.*[22] indicated that these interatomic distances are similar to those in m-ZrO_2. Stachs *et al.*[23] investigated structural parameters of two zirconia xerogels. It was found that local atomic ordering in the dried xerogel is similar to m-ZrO_2, it resembles t-ZrO_2[23] while in the xerogel annealed at $\approx$ 300 °C. Zirconium salts have a well defined structure, in comparison with hydrous zirconia, which enables an easier insight into the mechanism of t-ZrO_2 formation in the thermal decomposition of these salts.

In our previous paper[24] we investigated the thermal decomposition products of three different zirconium salts ($ZrOCl_2 \cdot 8\,H_2O$, $ZrO(NO_3)_2 \cdot 2\,H_2O$ and $Zr(SO_4)_2 \cdot 4\,H_2O$). It was shown that the transition from the starting salt to ZrO_2 proceeds through an amorphous intermediary. In all three cases, the first crystallization product contained, besides m-ZrO_2, metastable t-ZrO_2. However, the volume fraction of the metastable phase depended on the nature of the starting salt. The first crystallization products of $ZrO(NO_3)_2 \cdot 2\,H_2O$ and $Zr(SO_4)_2 \cdot 4\,H_2O$ salts contained m-ZrO_2 as dominant phase, while in the case of $ZrOCl_2 \cdot 8\,H_2O$ the first crystallization product contained metastable t-ZrO_2 as dominant phase with only traces of

m-ZrO_2.[24] The observed diversity could be a result of differences in the structural nature of the starting salts, in agreement with the model of Livage *et al.*[8] Similarity of the structural parameters (Zr–Zr and Zr–O distances) of the $ZrOCl_2 \cdot 8\,H_2O$ salt and of t-ZrO_2 supports this model.[25] However, the observed differences in the phase composition of the thermal decomposition products could result from the t-$ZrO_2 \rightarrow m$-ZrO_2 transition during the cooling to room temperature (RT). The presence of this kind of transition was revealed by *in situ* phase analysis of the crystallization products of hydrous zirconia.[26–28] It was found[27,28] that, regardless of precipitation pH, hydrous zirconia crystallized as metastable t-ZrO_2, which may or may not transform to m-ZrO_2 during cooling to RT.[17]

In the present work, we used high-temperature X-ray diffraction (XRD) to determine the phase composition of the thermal decomposition products of zirconium salts. On the basis of the results obtained, a mechanism of t-ZrO_2 formation was proposed.

EXPERIMENTAL

Zirconium salts $ZrO(NO_3)_2 \cdot 2\,H_2O$ (Ventron) and $Zr(SO_4)_2 \cdot 4\,H_2O$ (Hopkins & Williams Ltd.) were thermally decomposed by calcination at temperatures of 330 and 650 °C, respectively. A mixture of different zirconium nitrates (major components $Zr(OH)_2(NO_3)_2 \cdot 4.7\,H_2O$ and $ZrO(NO_3)_2 \cdot 2\,H_2O$) provided by Ventron were also thermally decomposed by calcination at 330 °C. All salts were calcinated for 2 hours in the presence of air. The samples obtained, designated Z1, Z2 and Z3, were characterized *in situ* by XRD using a Philips counter diffractometer, model MPD 1880, with monochromatized Cu-Kα radiation. The samples were deposited onto the platinum heating strip inside the high-temperature chamber (Paar HTK 10), attached to the diffractometer, and heated up to 1200 °C at a heating rate of 5 °C per minute. Heating was performed at a low air pressure of $\approx 2 \times 10^{-3}$ Pa, achieved using rotational and turbomolecular pumps. After reaching the final temperature (1200 °C), the samples were cooled to RT under the same pressure and the phase composition was determined. Afterwards, air was admitted into the chamber, and the phase composition was determined again after 24 hours. During the heating, diffraction data were collected at selected temperatures. Before starting data collection, samples were kept at the selected temperature for 10 minutes, while data collection took about 30 minutes. XRD patterns were scanned over the 2θ range from 20 to 38°, which contains the most prominent diffraction lines of m-ZrO_2 and t-ZrO_2 for Cu-Kα radiation. Data were collected in steps of 0.02° (2θ) with a fixed counting time of 5 s. The notation of samples and the results of phase analysis at the selected temperatures are given in Table I.

Additionally, sample Z2 was also calcinated for 1 hour at temperatures of 400, 500 and 700 °C. The calcination was performed at the atmospheric air pressure, and the phase composition was determined after cooling to RT.

TABLE I

The results of high-temperature X-ray diffraction study of samples Z1, Z2 and Z3,
obtained after the thermal decomposition of zirconium salts

Sample	Treatment	Phase composition (volume fractions)
Z1 $(ZrO(NO_3)_2 \cdot 2\,H_2O$ calcinatied at 330 °C in air, and then cooled to RT)	–	am
	350 °C	am
	375 °C	am + t-ZrO_2
	450 °C	t-ZrO_2 + am
	500 °C	t-ZrO_2
	550 °C	t-ZrO_2
	600 °C	t-ZrO_2
	650 °C	t-ZrO_2 + c-ZrO_2
	700 °C	t-ZrO_2 + c-ZrO_2
	800 °C	t-ZrO_2
	900 °C	t-ZrO_2
	1000 °C	t-ZrO_2
	1100 °C	t-ZrO_2
	1200 °C	t-ZrO_2
	– cooling from 1200 °C to RT and exposure to air at RT	m-ZrO_2 (0.75) + t-ZrO_2 (0.25)
Z1A (the same preparation procedure as for sample Z1)	600 °C	t-ZrO_2 + am
	1200 °C	t-ZrO_2
	– cooling from 1200 °C to RT	t-ZrO_2 (0.88) + m-ZrO_2 (0.12)
	– exposure to air at RT	m-ZrO_2 (0.54) + t-ZrO_2 (0.46)
Z2 (mixture of zirconium nitrates calcinated at 330 °C in air, and then cooled to RT)	–	am
	400 °C	am
	500 °C	am + t-ZrO_2
	600 °C	t-ZrO_2 + am
	800 °C	t-ZrO_2
	1000 °C	t-ZrO_2
	1200 °C	t-ZrO_2
	– cooling from 1200 °C to RT	t-ZrO_2 (0.89) + m-ZrO_2 (0.11)
	– exposure to air at RT	m-ZrO_2 (0.65) + t-ZrO_2 (0.35)
Z3 $(Zr(SO_4)_2 \cdot 4H_2O$ calcinated at 650 °C in air, and then cooled to RT)	–	am + ZS + t-ZrO_2 + m-ZrO_2
	500 °C	ZS + t-ZrO_2 + m-ZrO_2 + am
	600 °C	t-ZrO_2 (0.69) + m-ZrO_2 (0.31) + ZS
	700 °C	t-ZrO_2 (0.82) + m-ZrO_2 (0.18) + ZS
	800 °C	t-ZrO_2 (0.89) + m-ZrO_2 (0.11) + ZS
	900 °C	t-ZrO_2 (0.92) + m-ZrO_2 (0.08) + ZS
	1000 °C	t-ZrO_2 (0.90) + m-ZrO_2 (0.10)
	1200 °C	t-ZrO_2 (0.80) + m-ZrO_2 (0.20)
	– cooling from 1200 °C to RT	t-ZrO_2 (0.69) + m-ZrO_2 (0.31)
	– exposure to air at RT	m-ZrO_2 (0.55) + t-ZrO_2 (0.45)

Description: ZS = zirconium sulfate; am = amorphous.

Remark: Treatment of the samples includes successive calcination up to 1200 °C at low air pressure, cooling from 1200 °C to RT and exposure to air of atmospheric pressure at RT.

RESULTS AND DISCUSSION

The volume fractions of m-ZrO_2 and t-ZrO_2 were determined from the integrated intensities of diffraction lines $\bar{1}11$ and 111 of m-ZrO_2, and line 101 of t-ZrO_2, following the procedure proposed by Toraya et al.[29] The volume fractions of m-ZrO_2, v_m, and t-ZrO_2, v_t, are given by

$$v_m = \frac{1.311x}{1+0.311x} \,, \tag{1}$$

$$v_t = 1-v_m \,, \tag{2}$$

where x is

$$x = \frac{I_m(\bar{1}11) + I_m(111)}{I_m(\bar{1}11) + I_m(111) + I_t(101)} \,. \tag{3}$$

The crystallite size, D, was estimated using the Scherrer equation

$$D = \frac{0.9\lambda}{\beta \cdot \cos\theta} \,, \tag{4}$$

λ being the X-ray wavelength, θ the Bragg angle, β the pure full width of the diffraction line at half of its maximum intensity (FWHM). The values of β were found by applying a correction for the instrumental broadening and the broadening caused by thermal vibrations. The width of the α-SiO_2 diffraction line 112 was used for the correction of instrumental broadening, following the procedure given in the literature.[30] The temperature dependence of the FWHM of the m-ZrO_2 sample diffraction lines, obtained after thermal decomposition of $ZrO(NO_3)_2 \cdot 2H_2O$ salt at 1300 °C, was used to examine the influence of thermal vibrations on the FWHM. Integrated intensities and FWHM of the diffraction lines were determined using the individual profile fitting method (computer program PROFIT).[31,32]

The phase composition of samples Z1, Z2 and Z3 was determined at RT in the presence of air. Samples Z1 and Z2, calcinated at 330 °C, were amorphous. On the other hand, sample Z3, calcinated at 650 °C, contained faint diffraction lines of the starting zirconium salt. The presence of these diffraction lines indicated that the process of thermal decomposition was not completed. Besides the diffraction lines of the starting zirconium sulfate, sample Z3 also contained weak and broad diffraction lines typical of t-ZrO_2 and m-ZrO_2 (Table I).

Figure 1 shows X-ray powder diffraction patterns for sample Z1 recorded at temperatures between 350 and 1200 °C. The corresponding results of

the phase analysis are given in Table I. At 350 °C, sample Z1 was still amorphous. The first indication of a crystal phase appeared at 375 °C as diffraction line 101, typical of t-ZrO_2. With further increase of temperature, more diffraction lines of t-ZrO_2 appeared. Intensities of these diffraction lines in-
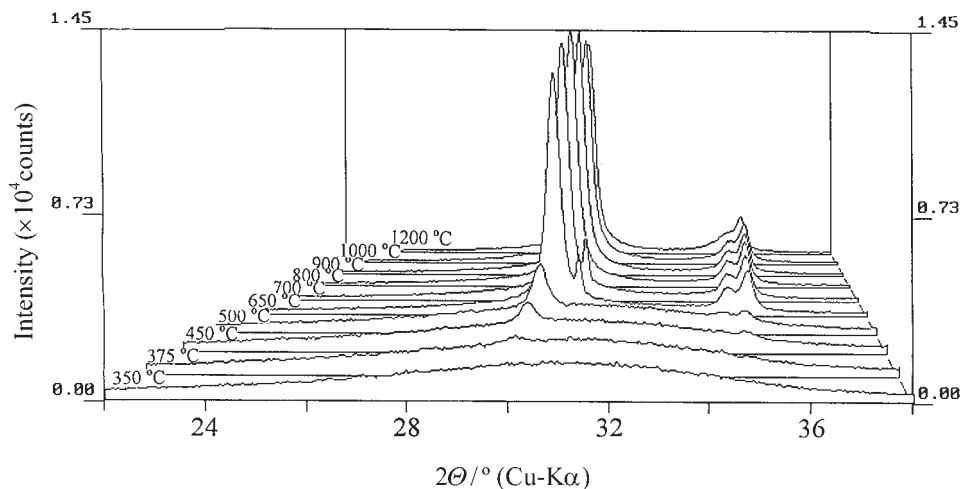

Figure 1. X-ray powder diffraction patterns for sample Z1 recorded at temperatures between 350 and 1200 °C.

creased, while the amorphous fraction maximum decreased. XRD patterns recorded at temperatures of 650 and 700 °C contained, besides the diffraction lines of t-ZrO_2, a weak diffraction line 111 of c-ZrO_2. At higher temperatures this diffraction line disappeared, and t-ZrO_2 was the only phase present. No sign of diffraction lines of the thermodynamically stable m-ZrO_2 phase could be observed.

These results depart considerably from the phase analysis results of the thermal decomposition products of $ZrO(NO_3)_2 \cdot 2\,H_2O$ salt obtained at RT in the presence of air.[24] The first crystallization product, obtained after calcination at 400 °C, contained approximately the same volume fractions of m-ZrO_2 and metastable t-ZrO_2. The fraction of metastable t-ZrO_2 decreased rapidly with an increase of temperature treatment due to the t-$ZrO_2 \rightarrow$ m-ZrO_2 transition. After calcination at 700 °C, the volume fraction of t-ZrO_2 was estimated at only 0.05.[24] On the other hand, *in situ* phase analysis of sample Z1 showed that no t-$ZrO_2 \rightarrow m$-ZrO_2 transition occurred during the heating up to 1200 °C. After cooling sample Z1 from 1200 °C to RT, m-ZrO_2

appeared and became the dominant phase, with the fraction of ≈ 0.75 (Table I). The cooling was performed at the low air pressure of $\approx 2 \times 10^{-3}$ Pa, inside the high-temperature chamber, but the XRD pattern was collected after exposure of the sample to air of atmospheric pressure ($\approx 10^5$ Pa). The fraction of t-ZrO_2 of ≈ 0.25 was much higher than that obtained after heating and cooling in the presence of air.[24]

In order to separate the effect of cooling from that of the exposure to air, the experiment with sample Z1 was repeated, but applying a shortened procedure. A new sample, denoted as Z1A, prepared by the same procedure as sample Z1, was heated only at 600 and 1200 °C and then cooled to RT. The shorter heating time resulted in broader diffraction lines. As in the previous experiment, at 1200 °C, only diffraction lines typical of t-ZrO_2 were present. However, asymmetry in the diffraction effect in the region of the diffraction line 101 of t-ZrO_2 indicates a possible superposition of the diffraction line 111 of c-ZrO_2. During cooling, partial transition from t-ZrO_2 to m-ZrO_2 occurred (Figure 2). After cooling to RT, the volume fraction of m-ZrO_2 at low air pressure ($\approx 2 \times 10^{-3}$ Pa) was estimated at 0.12. After a prolonged sample exposure to air of atmospheric pressure at RT, m-ZrO_2 became the dominant phase, having the fraction of 0.54. This result indicated that the presence of air (oxygen) supports the t-$ZrO_2 \rightarrow m$-ZrO_2 transition. A higher fraction of metastable t-ZrO_2 phase in the final product of sample Z1A (0.46) in comparison with that in the final product of sample Z1 (0.25) might be explained in terms of a much smaller crystallite size in sample Z1A than in sample Z1 (Table II).

Figure 3 shows X-ray powder diffraction patterns for sample Z2 recorded at temperatures between 350 and 1200 °C. The corresponding results of phase analysis are given in Table I. Similarly as in the case of sample Z1, the starting material was amorphous. The first indication of the crystal phase as a diffraction line 101 of t-ZrO_2 appeared at a temperature (500 °C) higher than for sample Z1. With further increase of temperature, more diffraction lines of t-ZrO_2 appeared and their intensities increased. Metastable t-ZrO_2 was the only phase present during the heating up to 1200 °C. After cooling from 1200 °C to RT, a partial transition of metastable t-ZrO_2 to m-ZrO_2 occurred (Figure 4). The volume fraction of m-ZrO_2 in the cooled sample at the air pressure of $\approx 2 \times 10^{-3}$ Pa was estimated to be 0.11. After the introduction of air at RT, the volume fraction of m-ZrO_2 increased significantly (estimated at 0.65).

The results of *in situ* phase analysis for sample Z2 were compared with those obtained at RT, after calcination and cooling of sample Z2 in the presence of air at atmospheric pressure (Figure 5). As in the case of the thermal
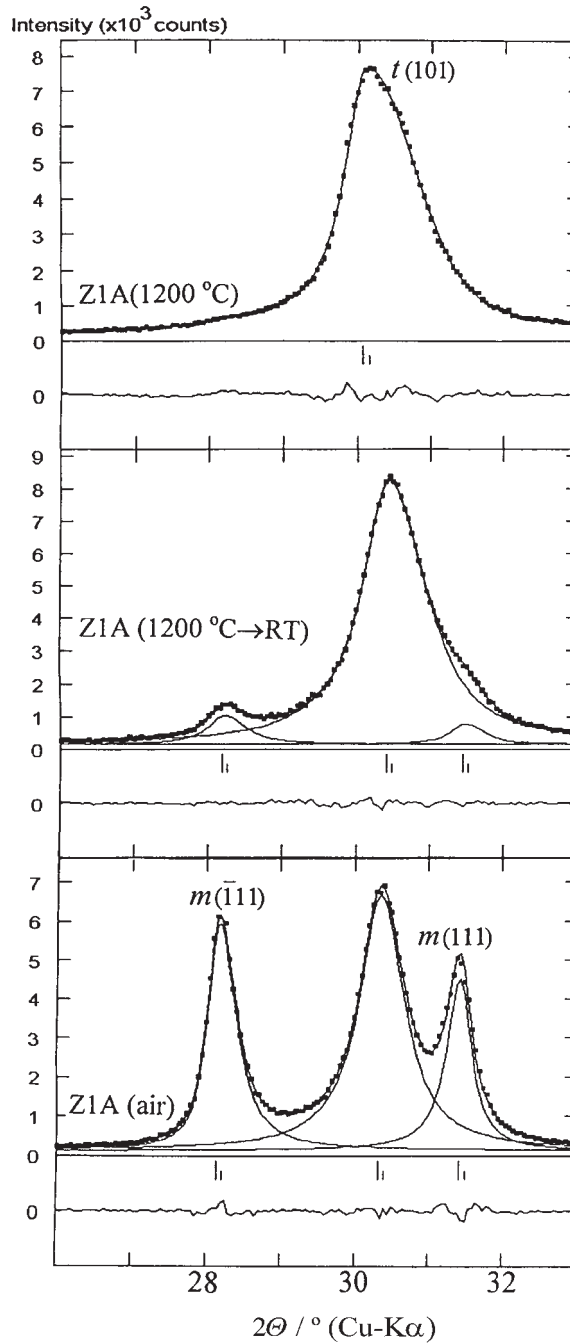
Figure 2. The results of individual profile fitting for sample Z1A recorded at 1200 °C
(a), after cooling from 1200 °C to RT (b) and after exposure to air at RT (c).
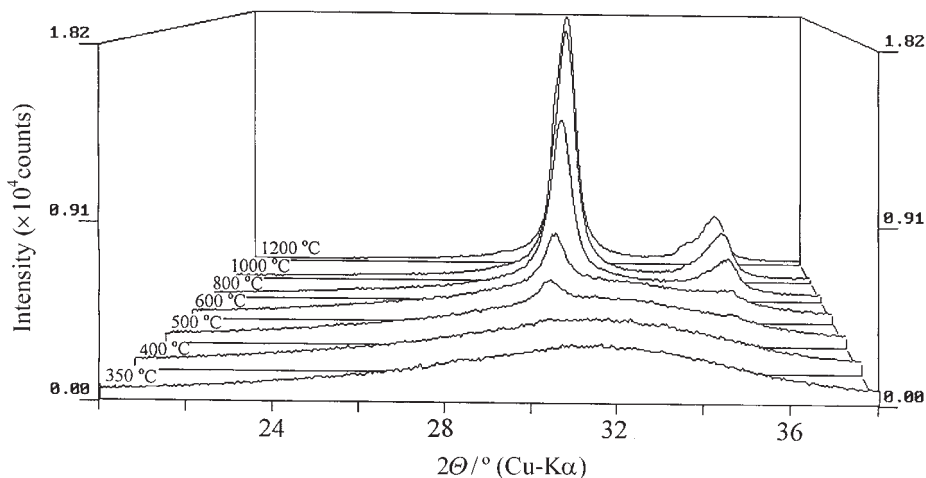
Figure 3. X-ray powder diffraction patterns for sample Z2 recorded at temperatures between 350 and 1200 °C.

decomposition of $ZrO(NO_3)_2 \cdot 2\,H_2O$,[24] the first crystallization product, obtained after calcination at 400 °C, contained both m-ZrO_2 and t-ZrO_2. However, in this case the volume fraction of m-ZrO_2 was much smaller (0.07). The volume fraction of m-ZrO_2 increased with an increase of temperature to 0.18, after calcination at 500 °C, and to 0.31, after calcination at 700 °C. These results differ from the results of *in situ* phase analysis which, for the corresponding temperatures, indicated the presence of t-ZrO_2 phase only.

The results of *in situ* phase analysis of sample Z3 are given in Table I. In contrast to samples Z1 and Z2, all XRD patterns of sample Z3 contained diffraction lines of both t-ZrO_2 and m-ZrO_2 phases. Diffraction lines of the starting zirconium sulfate were also present at temperatures up to ≈ 900 °C. An increase of temperature from 600 to 800 °C caused a decrease of diffraction line intensities of the starting salt, and an increase of those of t-ZrO_2 phase (Figure 6). Diffraction line intensities of m-ZrO_2 were approximately unchanged. These results indicated that t-ZrO_2 was the dominant crystalline product of the thermal decomposition of $Zr(SO_4)_2 \cdot 4\,H_2O$. After disappearance of the diffraction lines of starting salt (≈ 1000 °C), the increase of temperature caused an increase of the volume fraction of m-ZrO_2 (Table I).

Cooling of sample Z3 from 1200 °C to RT caused partial transition of metastable t-ZrO_2 to m-ZrO_2, as shown in Figure 7. After cooling, the volume fraction of m-ZrO_2 increased from 0.20 (at 1200 °C) to 0.31. Exposure of the sample to air of atmospheric pressure at RT caused a further increase of the m-ZrO_2 fraction, which became the dominant phase, estimated at 0.55.
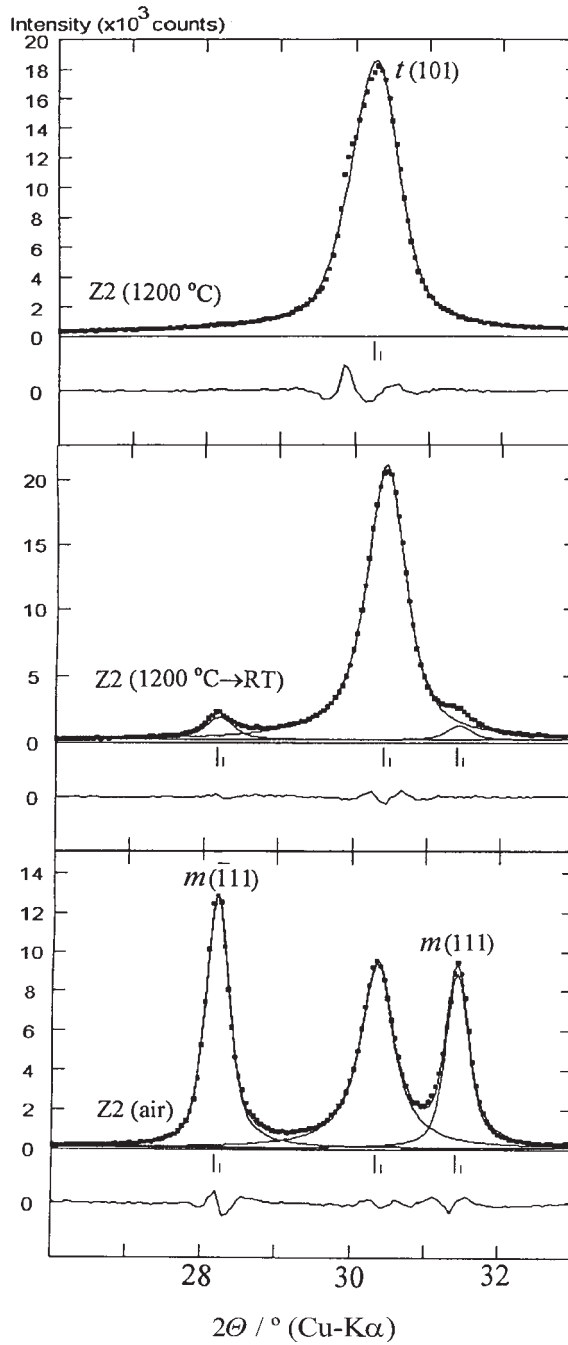
Figure 4. The results of individual profile fitting for sample Z2 recorded at 1200 °C (a), after cooling from 1200 °C to RT (b) and after exposure to air at RT (c).
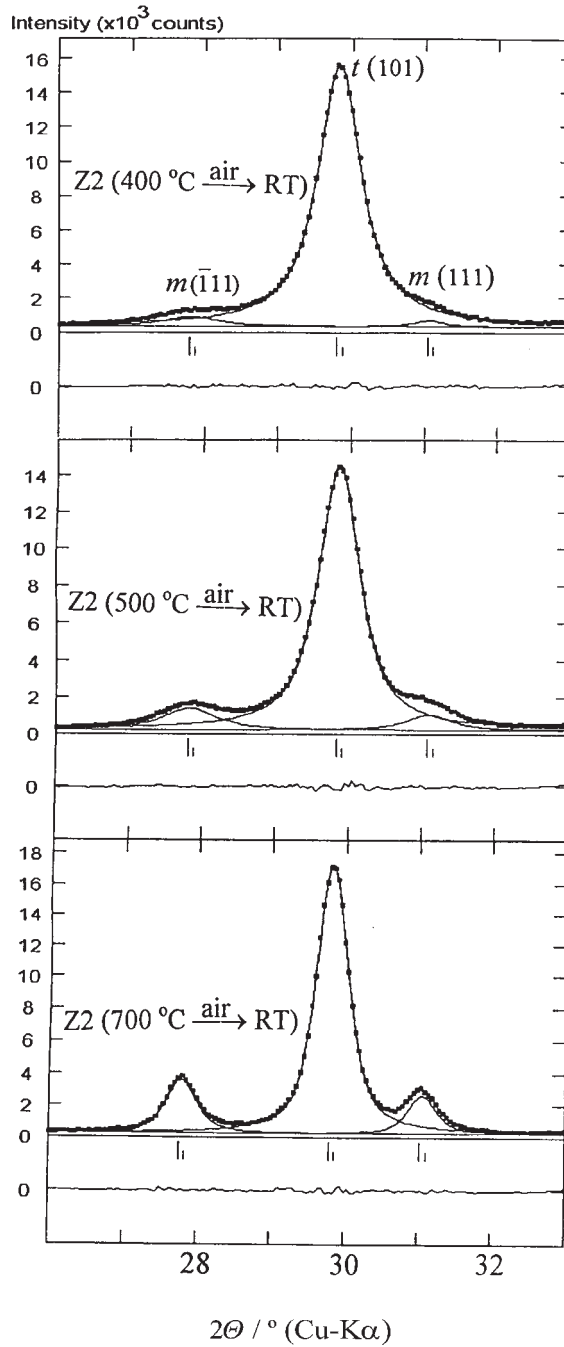
Figure 5. Characteristic parts of XRD patterns taken at RT from sample Z2 calcinated at 400, 500 and 700 °C in the presence of air.
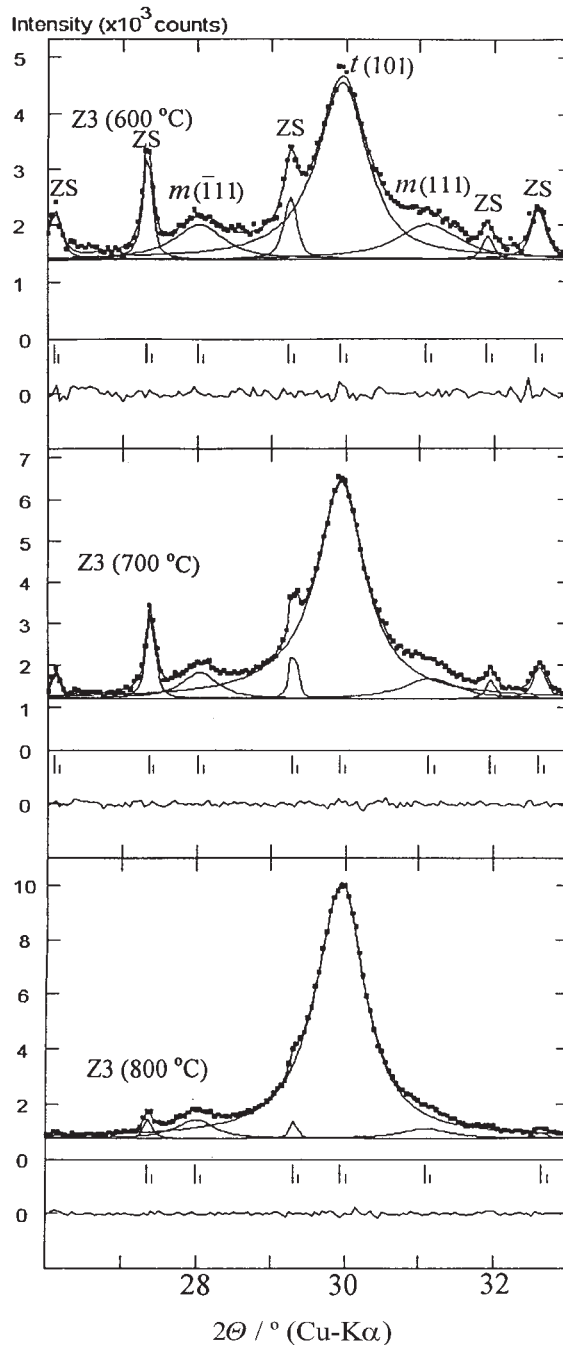
Figure 6. The results of individual profile fitting for sample Z3 recorded at temperatures of 600, 700 and 800 °C.
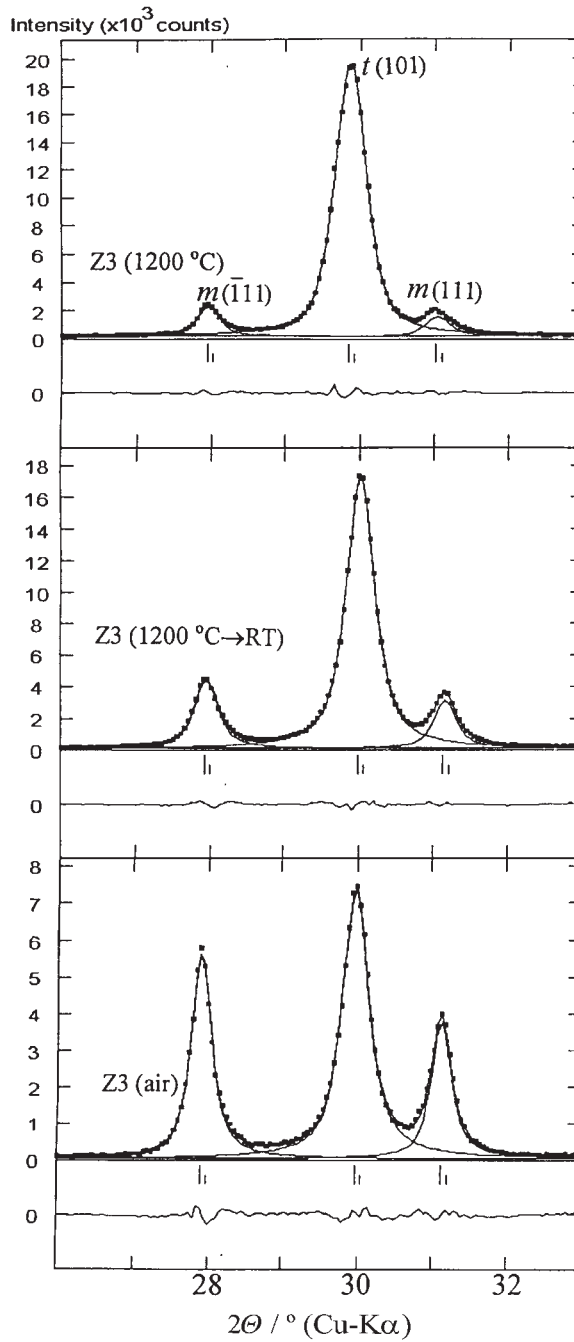
Figure 7. The results of individual profile fitting for sample Z3 recorded at 1200 °C (a), after cooling from 1200 °C to RT (b) and after exposure to air at RT (c).

Figure 8 shows the influence of temperature on the FWHM of the diffraction line 101 of t-ZrO_2. The corresponding values of FWHM and the estimated crystallite sizes are given in Table II. In the case of samples Z1A and Z3, the increase of temperature caused a decrease of the FWHM. In the case of sample Z1, the increase of temperature from 400 to 700 °C caused a decrease of the FWHM, but a further increase of temperature up to 1200 °C caused a gradual increase of the FWHM. A similar increase of the FWHM with increased temperature was observed for sample Z2. These results indicated that two opposite phenomena occurred during the temperature treatment. The first, which caused a decrease of FWHM, can be attributed to the crystal growth. The second, which caused an increase of FWHM, can be attributed to the influence of thermal vibrations and lattice defects. XRD analysis at high temperature of a well-crystallized m-ZrO_2 was performed at selected temperatures up to 1200 °C, in the same way as for the sample Z1. The obtained results indicated that the influence of thermal vibrations
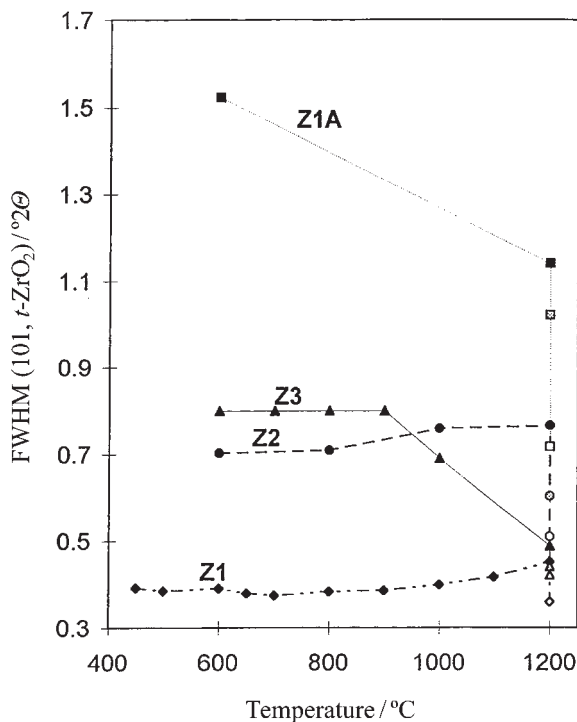

Figure 8. Influence of temperature on the FWHM of the diffraction line 101 of t-ZrO_2. Full symbols represent *in situ* obtained values of FWHM, half-empty symbols represent values obtained after cooling from 1200 °C to RT, and empty symbols represent values obtained after exposure to air at RT.

TABLE II

Influence of temperature on the FWHM of the diffraction line 101 of t-ZrO_2 and the diffraction line $\bar{1}11$ of m-ZrO_2 and the corresponding crystallite sizes, estimated using the Scherrer equation, of samples Z1, Z1A, Z2 and Z3

Sample	Treatment	FWHM / °2θ		Crystallite size / nm	
		t-ZrO_2	m-ZrO_2	t-ZrO_2	m-ZrO_2
	400 °C	0.456(86)	–	21.0	–
	450 °C	0.392(27)	–	25.4	–
	500 °C	0.385(12)	–	26.0	–
	550 °C	0.388(6)	–	25.9	–
	600 °C	0.391(4)	–	25.6	–
	650 °C	0.379(3)	–	26.5	–
Z1	700 °C	0.375(6)	–	26.7	–
	800 °C	0.383(4)	–	26.2	–
	900 °C	0.386(5)	–	26.0	–
	1000 °C	0.400(5)	–	24.9	–
	1100 °C	0.417(4)	–	23.7	–
	1200 °C	0.452(5)	–	21.3	–
	– cooling from 1200 °C to RT	–	–	–	–
	– exposure to air at RT	0.360(8)	0.382(6)	28.3	26.1
	600 °C	1.522(89)	–	5.8	–
Z1A	1200 °C	1.121(78)	–	7.9	–
	– cooling from 1200 °C to RT	1.030(11)	0.551(61)	8.6	16.9
	– exposure to air at RT	0.716(11)	0.434(57)	12.7	22.6
	600 °C	0.703(20)	–	13.0	–
	800 °C	0.709(6)	–	12.9	–
Z2	1000 °C	0.759(6)	–	12.0	–
	1200 °C	0.766(8)	–	11.9	–
	– cooling from 1200 °C to RT	0.604(5)	0.433(14)	15.3	22.4
	– exposure to air at RT	0.510(13)	0.362(33)	18.6	28.4
	700 °C	0.789(12)	0.572(51)	11.5	16.1
	800 °C	0.790(81)	0.573(44)	11.5	16.1
	900 °C	0.801(8)	0.621(37)	11.5	15.0
Z3	1000 °C	0.690(6)	0.465(19)	13.2	20.5
	1200 °C	0.489(10)	0.344(10)	19.5	29.9
	– cooling from 1200 °C to RT	0.441(5)	0.369(7)	22.0	27.5
	– exposure to air at RT	0.422(8)	0.304(6)	23.6	35.2
	–	–	0.321(5)	–	32.6
m-ZrO_2	1100 °C	–	0.325(5)	–	32.5
	1200 °C	0.221(11)	0.322(8)	57.8	32.6
	– cooling from 1200 °C to RT	–	0.320(8)	–	32.6

on the increase of FWHM is smaller than the effect observed after the cooling of samples (Table II). For all the samples studied, cooling from 1200 °C to RT caused a decrease of FWHM. Decrease of FWHM continued after exposure of samples to air of atmospheric pressure at RT. The influence of air was especially pronounced for sample Z1A (Table II). These results lead to the conclusion that the lattice defects related to oxygen vacancies prevented the crystal growth, but after exposure to air (oxygen) crystallite sizes increased (Table II). A similar conclusion was made by Osendi *et al.*[15] These authors concluded that the annealing of lattice defects favours both $t\text{-}ZrO_2 \rightarrow m\text{-}ZrO_2$ transition and crystal growth, so in this way the critical crystallite size, proposed by Garvie,[5] can be understood.

The results obtained indicated that the structural parameters of the starting zirconium salts were not the most important factor for $t\text{-}ZrO_2$ formation. On the other hand, the connection between the formation of $t\text{-}ZrO_2$ and the presence of oxygen vacancies was evident in all three cases. The presence of oxygen vacancies was found to be a key factor in the stabilization of high temperature ZrO_2 polymorphs in solid solutions with suitable oxides.[33,34] The strongly covalent nature of the Zr–O bond favours a 7-fold coordination of Zr^{4+} cation. High temperature ZrO_2 polymorphs, with an 8-fold coordination of Zr^{4+} cations, become stable when the average Zr^{4+} coordination number is reduced by dopant cations that introduce oxygen vacancies.[33] It can be concluded that the same mechanism caused stabilization of metastable $t\text{-}ZrO_2$, but in this case the oxygen vacancies were introduced into the ZrO_2 lattice during the process of calcination. The incorporation of oxygen, present in the surrounding atmosphere, into the ZrO_2 lattice causes the $t\text{-}ZrO_2 \rightarrow m\text{-}ZrO_2$ transition. Decrease of the oxygen content in the surrounding atmosphere or covering of the zirconia surface with substances, such as SO_4^{2-} or Cr_2O_3, that can strongly interact with the zirconia surface sites,[3,4,35] make transition to $m\text{-}ZrO_2$ more difficult.

A change of the local atomic ordering in the calcinated zirconia xerogels, from an $m\text{-}ZrO_2$-like to a $t\text{-}ZrO_2$-like one,[23] is probably also influenced by the introduction of oxygen vacancies. Stachs *et al.*[23] found that zirconia xerogel with structural parameters similar to $m\text{-}ZrO_2$ contained an excess of oxygen, which was lost at elevated temperature. During this process the oxygen vacancies can be introduced into the lattice, causing a change of the atomic arrangement in a way resembling that of $t\text{-}ZrO_2$.

CONCLUSION

The results of the *in situ* X-ray powder diffraction study at high temperature showed that amorphous precursors obtained after thermal decomposition of different zirconium salts crystallized to metastable $t\text{-}ZrO_2$, which

remained stable up to 1200 °C. A thermodynamically stable m-ZrO_2 phase appeared after cooling to RT. The content of metastable t-ZrO_2 in samples cooled to RT at low air pressure was much higher than in samples obtained after heating and cooling in the presence of air at atmospheric pressure ($\approx$ 10^5 Pa). The importance of oxygen for the advance of the t-$ZrO_2 \rightarrow m$-ZrO_2 transition indicated that the formation of metastable t-ZrO_2 was due to oxygen vacancies in the zirconia lattice. On the other hand, the structural nature of the starting materials seemed to have a minor influence on the formation of t-ZrO_2.

REFERENCES

1. I. Clark and D. H. Reynolds, *Ind. Eng. Chem.* **29** (1937) 711–715.
2. R. Cypres, R. Wollast, and J. Raucq, *Ber. Dtsch. Keram. Ges.* **40** (1963) 527–532.
3. R. Srinivasan, T. R. Watkins, C. R. Hubbard, and B. H. Davis, *Chem. Mater.* **7** (1995) 725–730.
4. G. Štefanić, S. Musić, S. Popović, and A. Sekulić, *J. Mol. Struct.* **408/409** (1997) 391–394.
5. R. C. Garvie, *J. Phys. Chem.* **69** (1965) 1238–1243.
6. R. C. Garvie and M. V. Swain, *J. Mater. Sci.* **20** (1985) 1193–1200.
7. E. Bailey, D. Lewis, Z. M. Librant, and L. J. Porter, *Trans. J. Br. Ceram. Soc.* **71** (1972) 25–30.
8. J. Livage, K. Doi, and C. Mazieres, *J. Am. Ceram. Soc.* **51** (1968) 349–353.
9. G. Keramidas and W. B. White, *J. Am. Ceram. Soc.* **57** (1974) 22–24.
10. E. Tani, M. Yoshimura, and S. Somiya, *J. Am. Ceram. Soc.* **66** (1983) 11–14.
11. T. Mitsuhasi, M. Ichihara, and U. Tatsuke, *J. Am. Ceram. Soc.* **57** (1974) 97–101.
12. Y. Murase and E. Kato, *J. Am. Ceram. Soc.* **62** (1979) 527.
13. Y. Murase and E. Kato, *J. Am. Ceram. Soc.* **66** (1983) 196–200.
14. J. Torralvo, M. A. Alario, and J. Soria, *J. Catal.* **86** (1984) 473–476.
15. I. Osendi, I. S. Moya, C. I. Serna, and I. Soria, *J. Am. Ceram. Soc.* **68** (1985) 135–139.
16. A. Clearfield, *J. Mater. Res.* **5** (1990) 161–162.
17. B. H. Davis, *J. Am. Ceram Soc.* **67** (1984) C–168.
18. R. Srinivasan, R. J. DeAngelis, and B. H. Davis, *J. Mater. Res.* **1** (1986) 583–588.
19. R. Srinivasan and B. H. Davis, *Catal. Lett.* **14** (1992) 165–170.
20. G. Štefanić, S. Popović, and S. Musić, *Thermochim. Acta* **303** (1997) 31–39.
21. Y. Zeng, G. Fagherazzi, F. Pinna, S. Polizzi, P. Riello, and M. Signoretto, *J. Non-Cryst. Solids* **155** (1993) 259–267.
22. Z. Yanwei, G. Fagherazzi, and S. Polizzi, *J. Mater. Sci.* **30** (1995) 2153–2158.
23. O. Stachs, Th. Gerber, and V. Petkov, *J. Non-Cryst. Solids* **210** (1997) 14–22.
24. G. Štefanić, S. Musić, S. Popović, and K. Furić, *Croat. Chem. Acta* **69** (1996) 223–239.
25. M. A. Blesa, A. J. G. Maroto, S. I. Passaggio, N. E. Figliolia, and G. Rigotti, *J. Mater. Sci.* **20** (1985) 4601–4609.
26. T. Mamott, P. Barnes, S. E. Tarling, S. L. Jones, and C. I. Norman, *J. Mater. Sci.* **26** (1991) 4054–4061.

27. R. Srinivasan, B. H. Davis, O. Burl Cavin, and C. R. Hubbard, *J. Am. Ceram. Soc*. **75** (1992) 1217–1222.
28. R. Srinivasan, C. R. Hubbard, O. B. Cavin, and B. H. Davis, *Chem. Mater.* **5** (1993) 27–31.
29. H. Toraya, M. Yoshimura, and S. Somiya, *J. Am. Ceram. Soc*. **67** (1984) C119–C121.
30. H. P. Klug and L. E. Alexander, *X-ray Diffraction Procedures*, 2nd edition, John Wiley & Sons, New York, 1974, pp. 640–642.
31. H. Toraya, *J. Appl. Crystallogr.* **19** (1986) 440–447.
32. B. Gržeta and H. Toraya, *Croat. Chem. Acta* **67** (1994) 273–288.
33. S. M. Ho, *Mater. Sci. Eng.* **54** (1982) 23–29.
34. P. Li, I.-W. Chen, and J. E. Penner-Hahn , *J. Am. Ceram. Soc*. **77** (1994) 118–128.
35. G. Štefanić, S. Popović, and S. Musić, *Mater. Lett.* **36** (1998) 240–244.

SAŽETAK

In situ fazna analiza produkata termičke razgradnje cirkonijevih soli

Goran Štefanić, Biserka Gržeta, Stanko Popović i Svetozar Musić

Rentgenskom difrakcijom u prahu pri visokoj temperaturi određen je fazni sastav produkata termičke razgradnje dviju cirkonijevih soli: $Zr(SO_4)_2 \cdot 4\ H_2O$ i $ZrO(NO_3)_2 \cdot 2\ H_2O$, te smjese cirkonijevih nitrata u kojoj su glavne komponente $Zr(OH)_2(NO_3)_2 \cdot 4,7\ H_2O$ i $ZrO(NO_3)_2 \cdot 2\ H_2O$. Uzorci su žareni do 1200 °C u visokotemperaturnoj komori vezanoj na difraktometar, pod tlakom zraka od $\approx 2 \times 10^{-3}$ Pa. Bez obzira na razliku u strukturi polaznih soli, primarni produkti termičke razgradnje kristalizirali su u t-ZrO_2, koji je ostao stabilan tijekom žarenja do 1200 °C. Taj rezultat pokazuje da struktura polaznog materijala nije najvažniji faktor nastanka metastabilnog t-ZrO_2. Termodinamički stabilan m-ZrO_2 pojavio se nakon hlađenja uzoraka na sobnu temperaturu. Ako je hlađenje provedeno pri niskom tlaku zraka, udio nastalog m-ZrO_2 bio je malen. Dovođenje zraka, čak i pri sobnoj temperaturi, uzrokuje znatan porast udjela m-ZrO_2, koji postaje dominantna faza. Važnost prisutnosti kisika za odvijanje prijalaza t-$ZrO_2 \rightarrow m$-ZrO_2 upućuje na uzročnu povezanost između nedostatka kisika u kristalnoj rešetki cirkonijeva dioksida i nastanka metastabilnog t-ZrO_2.